Appears in the Proceedings of IEEE GLOBECOM'07, November 2007.

A Three Dimensional Parametric Model for Wideband MIMO Mobile-to-Mobile Channels

Alenka G. Zajić and Gordon L. Stüber
School of Electrical and Computer Engineering
Georgia Institute of Technology, Atlanta, GA 30332 USA

***Abstract*— A three-dimensional (3-D) geometrical propagation model for wideband multiple-input multiple-output (MIMO) mobile-to-mobile (M-to-M) communications is proposed. Based on the geometrical model, a 3-D parametric reference model for wideband MIMO M-to-M multipath fading channels is developed. From the reference model, the space-time-frequency correlation function and the space-Doppler power spectral density are derived for a 3-D non-isotropic scattering environment. Finally, some simulation results are presented and compared with measured data. The close agreement between the theoretical and empirical curves confirms the utility of the proposed wideband model.**

I. Introduction

Mobile-to-mobile (M-to-M) radio propagation channels arise in inter-vehicular communications, mobile ad-hoc wireless networks, and relay-based cellular radio networks. The statistical properties of M-to-M channels are quite different from conventional fixed-to-mobile (F-to-M) cellular land mobile radio channels [1]. M-to-M communication systems are equipped with low elevation antennas and have both the transmitter ($\mathrm{T_x}$) and receiver ($\mathrm{R_x}$) in motion. Akki and Haber [1] proposed a reference model for single-input single-output (SISO) M-to-M Rayleigh fading channels. The reference models for narrowband multiple-input multiple-output (MIMO) M-to-M channels have been proposed in [2], [3]. All these models assume that the field incident on the $\mathrm{T_x}$ or $\mathrm{R_x}$ antenna array is composed of a number of waves travelling only in the *horizontal* plane. This assumption is acceptable only for certain environments, e.g., rural areas. However, it does not seem appropriate for an urban environment where the $\mathrm{T_x}$ and $\mathrm{R_x}$ antenna arrays are often located in close proximity to and lower than surrounding buildings. Recently, we proposed a three-dimensional (3-D) reference model for *narrowband* MIMO M-to-M multipath fading channels [4].

This paper presents a 3-D parametric reference model for *wideband* MIMO M-to-M channels. To describe our 3-D reference model, we first introduce a 3-D geometrical model for wideband MIMO M-to-M channels, referred to as the "concentric-cylinders" model. This model is extension of the "two-cylinder" model for M-to-M channels proposed in [4]. Previously reported models for narrowband MIMO M-to-M channels [2] - [4] consider radio propagation in outdoor macrocells, assuming that all rays are only double-bounced. This paper proposes a parametric reference model that employs the "concentric-cylinders" model and constructs the input delay-spread function as a superposition of the line-of-sight (LoS), single-bounced, and double-bounced rays. The parametric nature of the model makes it adaptable to a variety of propagation environments, i.e., outdoor micro- and macro-cells. From the new reference model, we derive a space-time-frequency correlation function (stf-cf) and a space-Doppler power spectral density (sD-psd) for a 3-D non-isotropic scattering environment. Finally, we present some simulation results for the sD-psd and compare them with measured data in [5]. The close agreement between the theoretical and empirical curves confirms the utility of the proposed wideband model.

The remainder of the paper is organized as follows. Section II introduces the geometrical "concentric-cylinders" model. Section III presents a 3-D parametric reference model for wideband MIMO M-to-M channels. Section IV derives the stf-cf and the sD-psd for 3-D non-isotropic scattering. Section V presents some simulation results to verify theoretical derivations. Finally, Section VI provides some concluding remarks.

II. A Geometrical "Concentric-Cylinders" Model

In this section, we introduce a 3-D geometrical model for wideband MIMO M-to-M channels, called the "concentric-cylinders" model. The "concentric-cylinders" model is an extension of the "two-cylinder" model for narrowband M-to-M channels proposed in [4]. We consider a wideband MIMO communication system with L_t transmit and L_r receive omnidirectional antenna elements. It is assumed that both the $\mathrm{T_x}$ and $\mathrm{R_x}$ are in motion and equipped with low elevation antennas. The radio propagation in outdoor micro- and macrocells is characterized by 3-D wide sense stationary uncorrelated scattering (WSSUS) with either line-of-sight (LoS) or non-line-of-sight (NLoS) conditions between the $\mathrm{T_x}$ and $\mathrm{R_x}$.

Fig. 1 shows the "concentric-cylinders" model with LoS, single- and double-bounced rays for a MIMO M-to-M channel with $L_t = L_r = 2$ antenna elements. This 2×2 antenna configuration will be used later to construct uniform linear antenna arrays with an arbitrary number of antennas. The "concentric-cylinders" model defines four cylinders, two around the $\mathrm{T_x}$ and another two around the $\mathrm{R_x}$, as shown in Fig. 1. Around

0
Prepared through collaborative participation in the Collaborative Technology Alliance for Communications & Networks sponsored by the U.S. Army Research Laboratory under Cooperative Agreement DAAD19-01-2-0011. The U.S. Government is authorized to reproduce and distribute reprints for Government purposes notwithstanding any copyright notation thereon.

the $\mathrm{T_x}$, M fixed omnidirectional scatterers occupy a volume between cylinders of radii R_{t1} and R_{t2}. It is assumed that the M scatterers lie on L cylindric surfaces of radii $R_{t1} \leq R_t^{(l)} \leq R_{t2}$, where $1 \leq l \leq L$. The l^{th} cylindric surface contains $M^{(l)}$ fixed omnidirectional scatterers, and the $(m,l)^{th}$ transmit scatterer is denoted by $S_T^{(m,l)}$. Similarly, around the $\mathrm{R_x}$, N fixed omnidirectional scatterers occupy a volume between cylinders of radii R_{r1} and R_{r2}. It is assumed that N scatterers lie on K cylindric surfaces of radii $R_{r1} \leq R_r^{(k)} \leq R_{r2}$, where $1 \leq k \leq K$. The k^{th} cylindric surface contains $N^{(k)}$ fixed omnidirectional scatterers, and the $(n,k)^{th}$ receive scatterer is denoted by $S_R^{(n,k)}$. The distance between the centers of the $\mathrm{T_x}$ and $\mathrm{R_x}$ cylinders is D. It is assumed that the radii R_{t2} and R_{r2} are much smaller than the distance D, i.e., $\max\{R_{t2}, R_{r2}\} \ll D$ (local scattering condition for outdoor micro- and macrocells). Furthermore, it is assumed that the distance D is smaller than $4R_{t1}R_{r1}L_r/(\lambda(L_t-1)(L_r-1))$ (channel does not experience keyhole behavior [6]), where λ denotes the carrier wavelength. The spacing between antenna elements at the $\mathrm{T_x}$ and $\mathrm{R_x}$ is denoted by d_T and d_R, respectively. It is assumed that d_T and d_R are much smaller than the radii R_{t1} and R_{r1}, i.e., $\max\{d_T, d_R\} \ll \min\{R_{t1}, R_{r1}\}$. Angles θ_T and θ_R describe the orientation of the $\mathrm{T_x}$ and $\mathrm{R_x}$ antenna array in the x-y plane, respectively, relative to the x-axis. Similarly, angles ψ_T and ψ_R describe the elevation of the $\mathrm{T_x}$'s antenna array and the $\mathrm{R_x}$'s antenna array relative to the x-y plane, respectively. The $\mathrm{T_x}$ and $\mathrm{R_x}$ are moving with speeds v_T and v_R in directions described by angles γ_T and γ_R, respectively. The symbols $\alpha_T^{(m,l)}$ and $\alpha_T^{(n,k)}$ are the azimuth

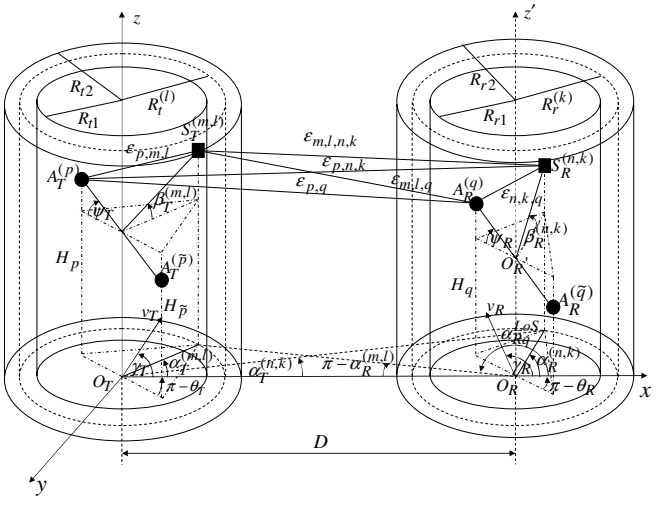

Fig. 1. The "concentric-cylinders" model with LoS, single- and double-bounced rays for a MIMO M-to-M channel with $L_t = L_r = 2$ antenna elements.

angles of departure (AAoD) of the waves that impinge on the scatterers $S_T^{(m,l)}$ and $S_R^{(n,k)}$, whereas $\alpha_R^{(m,l)}$ and $\alpha_R^{(n,k)}$ are the azimuth angles of arrival (AAoA) of the waves scattered from $S_T^{(m,l)}$ and $S_R^{(n,k)}$, respectively. Similarly, the symbols $\beta_T^{(m,l)}$ and $\beta_R^{(n,k)}$ denote the elevation angle of departure (EAoD) and the elevation angle of arrival (EAoA), respectively. The symbols $\epsilon_{p,m,l}$, $\epsilon_{m,l,q}$, $\epsilon_{p,n,k}$, $\epsilon_{n,k,q}$, $\epsilon_{m,l,n,k}$, and $\epsilon_{p,q}$ denote distances $A_T^{(p)}$ - $S_T^{(m,l)}$, $S_T^{(m,l)}$ - $A_R^{(q)}$, $A_T^{(p)}$ - $S_R^{(n,k)}$, $S_R^{(n,k)}$ - $A_R^{(q)}$, $S_T^{(m,l)}$ - $S_R^{(n,k)}$, and $A_T^{(p)}$ - $A_R^{(q)}$, respectively, as shown in Fig. 1. Finally, α_{Rq}^{LoS} denotes the AAoAs of the LoS paths.

III. A 3-D Parametric Model for Wideband MIMO Mobile-to-Mobile Channels

In this section, we derive a parametric reference model for wideband MIMO M-to-M multipath fading channels. The MIMO channel is described by an $L_r \times L_t$ matrix $\mathbf{H}(t,\tau) = [h_{ij}(t,\tau)]_{L_r \times L_t}$ of the input delay-spread functions. From the geometrical concentric-cylinders model, the input delay-spread function of the link $A_T^{(p)} - A_R^{(q)}$ is a superposition of the LoS, single-bounced, and double-bounced rays, and can be written as follows

$$h_{pq}(t,\tau) = h_{pq}^{SBT}(t,\tau) + h_{pq}^{SBR}(t,\tau) + h_{pq}^{DB}(t,\tau) + h_{pq}^{LoS}(t,\tau). \quad (1)$$

To simplify further derivations, we will use the time-variant transfer function instead of the input delay-spread function. The time-variant transfer function is defined as the Fourier transformation of the input delay-spread function and can be written as

$$\begin{aligned} T_{pq}(t,f) &= \mathcal{F}_\tau\{h_{pq}(t,\tau)\} = T_{pq}^{SBT}(t,f) + T_{pq}^{SBR}(t,f) \\ &+ T_{pq}^{DB}(t,f) + T_{pq}^{LoS}(t,f). \end{aligned} \quad (2)$$

The single-bounced components of the time-variant transfer function are, respectively,

$$T_{pq}^{SBT}(t,f) = \sqrt{\eta_T} \lim_{M\to\infty} \sum_{l=1}^{L} \sum_{m=1}^{M^{(l)}} \xi_{m,l} g_{m,l}(t) e^{-j2\pi f \tau_{m,l}}, \quad (3)$$

$$T_{pq}^{SBR}(t,f) = \sqrt{\eta_R} \lim_{N\to\infty} \sum_{k=1}^{K} \sum_{n=1}^{N^{(k)}} \xi_{n,k} g_{n,k}(t) e^{-j2\pi f \tau_{n,k}}, \quad (4)$$

where parameters $\xi_{m,l}$, $\xi_{n,k}$, $\tau_{m,l}$, and $\tau_{n,k}$ denote amplitudes of the multipath components and time delays, respectively. Functions $g_{m,l}(t)$ and $g_{n,k}(t)$ are defined as follows

$$\begin{aligned} g_{m,l}(t) &= e^{-j\frac{2\pi}{\lambda}(\epsilon_{p,m,l}+\epsilon_{m,l,q})} \\ &e^{j2\pi t\left[f_{T\max}\cos\left(\alpha_T^{(m,l)}-\gamma_T\right)+f_{R\max}\cos\left(\alpha_R^{(m,l)}-\gamma_R\right)\right]+j\phi_{m,l}}, \end{aligned} \quad (5)$$

$$\begin{aligned} g_{n,k}(t) &= e^{-j\frac{2\pi}{\lambda}(\epsilon_{p,n,k}+\epsilon_{n,k,q})} \\ &e^{j2\pi t\left[f_{T\max}\cos\left(\alpha_T^{(n,k)}-\gamma_T\right)+f_{R\max}\cos\left(\alpha_R^{(n,k)}-\gamma_R\right)\right]+j\phi_{n,k}}, \end{aligned} \quad (6)$$

where $f_{T\max} = v_T/\lambda$ and $f_{R\max} = v_R/\lambda$ are the maximum Doppler frequencies associated with the $\mathrm{T_x}$ and $\mathrm{R_x}$, respectively, and λ is the carrier wavelength. The amplitudes $\xi_{m,l}$ and $\xi_{n,k}$ are approximated as

$$\xi_{m,l} \approx \frac{\Omega_{pq}\left(1-\frac{\gamma}{2}\frac{R_t^{(l)}}{D}\right)}{\sqrt{M(K_{pq}+1)}}, \quad \xi_{n,k} \approx \frac{\Omega_{pq}\left(1-\frac{\gamma}{2}\frac{R_r^{(k)}}{D}\right)}{\sqrt{N(K_{pq}+1)}}, \quad (7)$$

where $\Omega_{pq} = D^{-\gamma/2}\sqrt{P_{pq}}\lambda/4\pi$, P_{pq} is the power transmitted through the subchannel $A_T^{(p)} - A_R^{(q)}$, K_{pq} is the Rice factor of

the subchannel $A_T^{(p)}$ -$A_R^{(q)}$, and γ is the path loss exponent. Finally, the time delays $\tau_{m,l}$ and $\tau_{n,k}$ are defined as the travel times of the waves scattered from the scatterers $S_T^{(m,l)}$ and $S_R^{(n,k)}$, i.e. $\tau_{m,l} = D/c_0 + R_t^{(l)}(1-\cos\alpha_T^{(m,l)})/c_0\cos\beta_T^{(m,l)}$ and $\tau_{n,k} = D/c_0 + R_r^{(k)}(1+\cos\alpha_R^{(n,k)})/c_0\cos\beta_R^{(n,k)}$, respectively, where c_0 is the speed of light. The double-bounced component of the time-variant transfer function is

$$T_{pq}^{DB}(t,f) = \sqrt{\eta_{TR}}\lim_{M,N\to\infty}\sum_{l,m=1}^{L,M^{(l)}}\sum_{k,n=1}^{K,N^{(k)}}\xi_{m,l,n,k}g_{m,l,n,k}(t)e^{-j2\pi f\tau_{m,l,n,k}}, \quad (8)$$

where $\xi_{m,l,n,k}$ and $\tau_{m,l,n,k}$ are the amplitude of the multipath component and the time delay, respectively. The function $g_{m,l,n,k}(t)$ is defined as

$$g_{m,l,n,k}(t) = e^{-j\frac{2\pi}{\lambda}(\epsilon_{p,m,l}+\epsilon_{m,l,n,k}+\epsilon_{n,k,q})+j\phi_{m,l,n,k}} e^{j2\pi t\left[f_{T\max}\cos\left(\alpha_T^{(m,l)}-\gamma_T\right)+f_{R\max}\cos\left(\alpha_R^{(n,k)}-\gamma_R\right)\right]}. \quad (9)$$

The amplitude $\xi_{m,l,n,k}$ is approximated as

$$\xi_{m,l,n,k} \approx \frac{\Omega_{pq}}{\sqrt{MN(K_{pq}+1)}}\left(1-\frac{\gamma}{2}\frac{R_t^{(l)}+R_r^{(k)}}{2D}\right). \quad (10)$$

The time delay $\tau_{m,l,n,k}$ is defined as the travel time of the wave impinged on the scatterer $S_T^{(m,l)}$ and scattered from the scatterer $S_R^{(n,k)}$, i.e. $\tau_{m,l,n,k} = D/c_0 + R_t^{(l)}(1-\cos\alpha_T^{(m,l)})/c_0\cos\beta_T^{(m,l)} + R_r^{(k)}(1+\cos\alpha_R^{(n,k)})/c_0\cos\beta_R^{(n,k)}$. Parameters η_T, η_R, and η_{TR} specify how much the single- and double-bounced rays contribute in the total power P_{pq}, i.e., these parameters satisfy $\eta_T+\eta_R+\eta_{TR}=1$. It is assumed that the angles of departure ($\alpha_T^{(m,l)}$ and $\beta_T^{(m,l)}$), the angles of arrival ($\alpha_R^{(n,k)}$ and $\beta_R^{(n,k)}$), and the radii $R_t^{(l)}$ and $R_r^{(k)}$ are random variables, and that the angles of departure and radii $R_t^{(l)}$ are independent from the angles of arrival and radii $R_r^{(k)}$. Note that the AAoA, $\alpha_R^{(m,l)}$, is a function of the AAoD, $\alpha_T^{(m,l)}$, and the AAoD, $\alpha_T^{(n,k)}$, is a function of the AAoA, $\alpha_R^{(n,k)}$ and, hence, they are not independent angular variables. Additionally, it is assumed that the phases $\phi_{m,l}$, $\phi_{n,k}$, and $\phi_{m,l,n,k}$ are random variables uniformly distributed on the interval $[-\pi,\pi)$ and independent from the angles of departure, the angles of arrival, and the radii of the cylinders. The LoS component of the time-variant transfer function is

$$T_{pq}^{LoS}(t,f) = \sqrt{\frac{K_{pq}}{K_{pq}+1}}\xi_{LoS}g_{LoS}(t)e^{-j2\pi f\tau_{LoS}}, \quad (11)$$

where $\xi_{LoS} \approx \Omega_{pq}$, $\tau_{LoS} = \sqrt{D^2+\Delta H^2}/c_0$, $g^{LoS}(t) = e^{j2\pi t[f_{R\max}\cos(\alpha_{Rq}^{LoS}-\gamma_R)+f_{T\max}\cos(\pi-\alpha_{Rq}^{LoS}-\gamma_T)]-j\frac{2\pi}{\lambda}\epsilon_{p,q}}$, and $\Delta H = (H_p - H_{\tilde{p}} - H_q + H_{\tilde{q}})/2$. Finally, the distances $\epsilon_{m,l,q}$, $\epsilon_{p,n,k}$, $\epsilon_{p,m,l}$, $\epsilon_{n,k,q}$, $\epsilon_{m,l,n,k}$, and $\epsilon_{p,q}$ can be expressed as functions of the random variables $\alpha_T^{(m,l)}$, $\beta_T^{(m,l)}$, $\alpha_R^{(n,k)}$, $\beta_R^{(n,k)}$, α_{Rq}^{LoS}, $R_t^{(l)}$, and $R_r^{(k)}$ as follows:

$$\epsilon_{m,l,q} \approx D-(0.5L_r+0.5-q)(d_{Ry}\Delta_T^{(l)}\sin\alpha_T^{(m,l)}-d_{Rx}),$$
$$\epsilon_{p,n,k} \approx D-(0.5L_t+0.5-p)(d_{Ty}\Delta_R^{(k)}\sin\alpha_R^{(n,k)}+d_{Tx}),$$
$$\epsilon_{p,m,l} \approx R_t^{(l)}-(0.5L_t+0.5-p)\big[d_{Tz}\sin\beta_T^{(m,l)}+d_{Tx}\cos\alpha_T^{(m,l)}\cos\beta_T^{(m,l)}+d_{Ty}\sin\alpha_T^{(m,l)}\cos\beta_T^{(m,l)}\big],$$
$$\epsilon_{n,k,q} \approx R_r^{(k)}-(0.5L_r+0.5-q)\big[d_{Rz}\sin\beta_R^{(n,k)}+d_{Rx}\cos\alpha_R^{(n,k)}\cos\beta_R^{(n,k)}+d_{Ry}\sin\alpha_R^{(n,k)}\cos\beta_R^{(n,k)}\big],$$
$$\epsilon_{m,l,n,k} \approx D,$$
$$\epsilon_{p,q} \approx D-(0.5L_t+0.5-p)d_{Tx}-(0.5L_r+0.5-q)d_R\cos\psi_R\cos(\alpha_{Rq}^{LoS}-\theta_R), \quad (12)$$

where parameters p and q take values from the sets $p\in\{1,\ldots,L_t\}$ and $q\in\{1,\ldots,L_r\}$, $d_{Tx} = d_T\cos\psi_T\cos\theta_T$, $d_{Ty} = d_T\cos\psi_T\sin\theta_T$, $d_{Rx} = d_R\cos\psi_R\cos\theta_R$, $d_{Ry} = d_R\cos\psi_R\sin\theta_R$, $d_{Tz} = d_T\sin\psi_T$, $d_{Rz} = d_R\sin\psi_R$, $\Delta_T^{(l)} = R_t^{(l)}/D$, and $\Delta_R^{(k)} = R_r^{(k)}/D$. Derivations of the expressions in (12) are omitted for brevity.

IV. Space-Time-Frequency Correlation Function and Space-Doppler Power Spectrum of the 3-D Reference Model

The normalized space-time-frequency correlation function between two time-variant transfer functions $T_{pq}(t,f)$ and $T_{\tilde{p}\tilde{q}}(t,f)$ is defined as

$$R_{pq,\tilde{p}\tilde{q}}(\Delta t,\Delta f) = \frac{\mathrm{E}\left[T_{pq}(t,f)^* T_{\tilde{p}\tilde{q}}(t+\Delta t,f+\Delta f)\right]}{\sqrt{\mathrm{E}[|T_{pq}(t,f)|^2]\mathrm{E}[|T_{\tilde{p}\tilde{q}}(t,f)|^2]}}, \quad (13)$$

where $(\,\cdot\,)^*$ denotes complex conjugate operation, $\mathrm{E}[\,\cdot\,]$ is the statistical expectation operator, $p,\tilde{p}\in\{1,\ldots,L_t\}$, and $q,\tilde{q}\in\{1,\ldots,L_r\}$. Since the number of local scatterers in the reference model is infinite, the discrete AAoDs, $\alpha_T^{(m,l)}$, EAoDs, $\beta_T^{(m,l)}$, AAoAs, $\alpha_R^{(n,k)}$, EAoAs, $\beta_R^{(n,k)}$, and radii $R_t^{(l)}$ and $R_r^{(k)}$ can be replaced with continuous random variables α_T, β_T, α_R, β_R, R_t, and R_r. To characterize the random azimuth angles α_T and α_R, we use the von Mises probability density function (pdf) defined as [7] $f(\theta) = \exp[k\cos(\theta-\mu)]/2\pi I_0(k)$, where $\theta\in[-\pi,\pi)$, $I_0(\,\cdot\,)$ is the zeroth-order modified Bessel function of the first kind, $\mu\in[-\pi,\pi)$ is the mean angle at which the scatterers are distributed in the x–y plane, and k controls the spread of scatterers around the mean. To characterize the random elevation angles β_T and β_R, we use the pdf [8]

$$f(\varphi) = \begin{cases} \frac{\pi}{4|\varphi_m|}\cos\left(\frac{\pi}{2}\frac{\varphi}{\varphi_m}\right), & |\varphi|\le|\varphi_m|\le\frac{\pi}{2} \\ 0, & \text{otherwise} \end{cases}, \quad (14)$$

where φ_m is the maximum elevation angle and lies in the range $0^\circ \le |\varphi_m| \le 20^\circ$ [9]. Such elevation angles are typical for "street-canyon" propagation, which is prevalent in M-to-M communications (e.g., two vehicles driving along streets)[1]. To characterize the radii R_t and R_r, we use the pdfs $f(R_t) = 2R_t/(R_{t2}^2-R_{t1}^2)$ and $f(R_r) = 2R_r/(R_{r2}^2-R_{r1}^2)$, respectively. Using trigonometric transformations, the equality $\int_{-\pi}^{\pi}\exp\{a\sin(c)+b\cos(c)\}dc = 2\pi I_0\left(\sqrt{a^2+b^2}\right)$

[1]Note that elevation angles higher than 20° have been found for "over the roof" propagation [9], which is characteristic for fixed-to-mobile cellular communications where the base-station is elevated above the roofs of buildings.

[10, eq. 3.338-4], and the results in [4], the stf-cfs of the single- and double-bounced components can be closely approximated as

$$R^{SBT}_{pq,\tilde{p}\tilde{q}}(d_T,d_R,\Delta t,\Delta f)\approx \tag{15}$$
$$\frac{\eta_T}{I_0(k_T)}\frac{\cos\left(\frac{2\pi}{\lambda}\beta_{Tm}d_{Tz}\right)}{1-\left(\frac{4\beta_{Tm}d_{Tz}}{\lambda}\right)^2}e^{-j\frac{2\pi}{\lambda}(q-\tilde{q})d_{Rx}}e^{-j2\pi\Delta t f_{R\max}\cos\gamma_R}$$
$$\int_{R_{t1}}^{R_{t2}}I_0\left(\sqrt{x^2_{SBT}+y^2_{SBT}}\right)\frac{2R_t\left(1-\gamma\frac{R_t}{D}\right)e^{-j\frac{2\pi}{c_0}\Delta f(D+R_t)}}{R^2_{t2}-R^2_{t1}}dR_t,$$
$$R^{SBR}_{pq,\tilde{p}\tilde{q}}(d_T,d_R,\Delta t,\Delta f)\approx \tag{16}$$
$$\frac{\eta_R}{I_0(k_R)}\frac{\cos\left(\frac{2\pi}{\lambda}\beta_{Rm}d_{Rz}\right)}{1-\left(\frac{4\beta_{Rm}d_{Rz}}{\lambda}\right)^2}e^{j\frac{2\pi}{\lambda}(p-\tilde{p})d_{Tx}}e^{j2\pi\Delta t f_{T\max}\cos\gamma_T}$$
$$\int_{R_{r1}}^{R_{r2}}I_0\left(\sqrt{x^2_{SBR}+y^2_{SBR}}\right)\frac{2R_r\left(1-\gamma\frac{R_r}{D}\right)e^{-j\frac{2\pi}{c_0}\Delta f(D+R_r)}}{R^2_{r2}-R^2_{r1}}dR_r,$$
$$R^{DB}_{pq,\tilde{p}\tilde{q}}(d_T,d_R,\Delta t,\Delta f)\approx \tag{17}$$
$$A_{DB}\int_{R_{t1}}^{R_{t2}}e^{-j\frac{2\pi}{c_0}\Delta f R_t}R_tI_0\left(\sqrt{x^2_{DB}+y^2_{DB}}\right)dR_t$$
$$\times\quad\int_{R_{r1}}^{R_{r2}}e^{-j\frac{2\pi}{c_0}\Delta f R_r}R_rI_0\left(\sqrt{w^2_{DB}+z^2_{DB}}\right)\left(1-\gamma\frac{R_r}{D}\right)dR_r+$$
$$A_{DB}\int_{R_{r1}}^{R_{r2}}e^{-j\frac{2\pi}{c_0}\Delta f R_r}R_rI_0\left(\sqrt{w^2_{DB}+z^2_{DB}}\right)dR_r$$
$$\times\quad\int_{R_{t1}}^{R_{t2}}e^{-j\frac{2\pi}{c_0}\Delta f R_t}R_tI_0\left(\sqrt{x^2_{DB}+y^2_{DB}}\right)\left(1-\gamma\frac{R_t}{D}\right)dR_t,$$

where $x_{SBT}\approx j2\pi[(p-\tilde{p})d_{Tx}/\lambda+\Delta t f_{T\max}\cos\gamma_T+\Delta f R_t/c_0]+k_T\cos\mu_T$, $y_{SBT}\approx j2\pi[(p-\tilde{p})d_{Ty}/\lambda+(q-\tilde{q})d_{Ry}\Delta_T/\lambda+\Delta t f_{T\max}\sin\gamma_T+\Delta t f_{R\max}\Delta_T\sin\gamma_R]+k_T\sin\mu_T$, $x_{SBR}\approx j2\pi[(q-\tilde{q})d_{Rx}/\lambda+\Delta t f_{R\max}\cos\gamma_R-\Delta f R_r/c_0]+k_R\cos\mu_R$, $y_{SBR}\approx j2\pi[(q-\tilde{q})d_{Ry}/\lambda+(p-\tilde{p})d_{Ty}\Delta_R/\lambda+\Delta t f_{R\max}\sin\gamma_R+\Delta t f_{T\max}\Delta_R\sin\gamma_T]+k_R\sin\mu_R$, $x_{DB}\approx j2\pi[(p-\tilde{p})d_{Tx}/\lambda+\Delta t f_{T\max}\cos\gamma_T+\Delta f R_t/c_0]+k_T\cos\mu_T$, $y_{DB}\approx j2\pi[(p-\tilde{p})d_{Ty}/\lambda+\Delta t f_{T\max}\sin\gamma_T]+k_T\sin\mu_T$, $z_{DB}\approx j2\pi[(q-\tilde{q})d_{Rx}/\lambda+\Delta t f_{R\max}\cos\gamma_R-\Delta f R_r/c_0]+k_R\cos\mu_R$, $w_{DB}\approx j2\pi[(q-\tilde{q})d_{Ry}/\lambda+\Delta t f_{R\max}\sin\gamma_R]+k_R\sin\mu_R$, and $A_{DB}=\eta_{TR}\cos(2\pi\beta_{Tm}d_{Tz}/\lambda)\cos(2\pi\beta_{Rm}d_{Rz}/\lambda)2e^{-j2\pi\Delta f D/c_0}/I_0(k_T)I_0(k_R)(1-(4\beta_{Tm}d_{Tz}/\lambda)^2)(1-(4\beta_{Rm}d_{Rz}/\lambda)^2)(R^2_{t2}-R^2_{t1})(R^2_{r2}-R^2_{r1})$. The integrals in (15) - (17) must be evaluated numerically, because they do not have closed-form solutions. Using (11) and approximation $\alpha^{LoS}_{Rq}=\alpha^{LoS}_{R\tilde{q}}\approx\pi$, the stf-cf of the LoS component can be approximated as

$$R^{LoS}_{pq,\tilde{p}\tilde{q}}(d_T,d_R,\Delta t,\Delta f)\approx\sqrt{K_{pq}K_{\tilde{p}\tilde{q}}}e^{j\frac{2\pi}{\lambda}[(p-\tilde{p})d_{Tx}-(q-\tilde{q})d_{Rx}]}$$
$$e^{j2\pi\Delta t[f_{T\max}\cos\gamma_T-f_{R\max}\cos\gamma_R]-\frac{2\pi}{c_0}\Delta f\sqrt{D^2+\Delta H^2}}. \tag{18}$$

Finally, the normalized stf-cf between two time-variant transfer functions $T_{pq}(t,f)$ and $T_{\tilde{p}\tilde{q}}(t,f)$ becomes a summation of the stf-cfs in (15) - (18).

The space-Doppler power spectral density (sD-psd) of the time-variant transfer function is the Fourier transformation of the space-time correlation function $R_{pq,\tilde{p}\tilde{q}}(d_T,d_R,\Delta t,\Delta f=0)$. Using the equality [10, eq. 6.677-3] and after extensive calculations, the sD-psds of the single-bounced components become

$$\mathcal{F}_{\Delta t}\{R^{SBT}_{pq,\tilde{p}\tilde{q}}(d_T,d_R,\Delta t,0)\}=\frac{\eta_T}{I_0(k_T)}\frac{\cos\left(\frac{2\pi}{\lambda}\beta_{T_m}d_{Tz}\right)}{1-\left(\frac{4\beta_{T_m}d_{Tz}}{\lambda}\right)^2}$$
$$\frac{\exp\{j2\pi(\nu+f_{R\max}\cos\gamma_R)A_{SBT}-j2\pi p_{x_{SBR}}\}}{\pi f_{T\max}\sqrt{1-[(\nu+f_{R\max}\cos\gamma_R)/f_{T\max}]^2}}I_{SBT}$$
$$\cosh\left[B_{SBT}\sqrt{1-[(\nu+f_{R\max}\cos\gamma_R)/f_{T\max}]^2}\right], \tag{19}$$
$$\mathcal{F}_{\Delta t}\{R^{SBR}_{pq,\tilde{p}\tilde{q}}(d_T,d_R,\Delta t,0)\}=\frac{\eta_R}{I_0(k_R)}\frac{\cos\left(\frac{2\pi}{\lambda}\beta_{R_m}d_{Rz}\right)}{1-\left(\frac{4\beta_{R_m}d_{Rz}}{\lambda}\right)^2}$$
$$\frac{\exp\{j2\pi(\nu-f_{T\max}\cos\gamma_T)A_{SBR}+j2\pi p_{x_{SBT}}\}}{\pi f_{R\max}\sqrt{1-[(\nu-f_{T\max}\cos\gamma_T)/f_{R\max}]^2}}I_{SBR}$$
$$\cosh\left[B_{SBR}\sqrt{1-[(\nu-f_{T\max}\cos\gamma_T)/f_{R\max}]^2}\right], \tag{20}$$

where $\mathcal{F}\{\ \cdot\ \}$ denotes the Fourier transformation, $\cosh(\ \cdot\ )$ is the hyperbolic cosine, $|\nu+f_{R\max}\cos\gamma_R|\le f_{T\max}$ and $|\nu-f_{T\max}\cos\gamma_T|\le f_{R\max}$. Parameters in equations (19) and (20) are defined as follows: $A_{SBT}=(2\pi p_{x_{SBT}}q_{x_{SBT}}+2\pi p_{y_{SBT}}q_{y_{SBT}}-w_{x_{SBT}})/2\pi f_{T\max}$, $B_{SBT}=k_T\sin(\mu_T-\gamma_T)+j2\pi p_{x_{SBT}}q_{y_{SBT}}-j2\pi p_{y_{SBT}}q_{x_{SBT}})$, $p_{x_{SBT}}=(p-\tilde{p})d_{Tx}/\lambda$, $q_{x_{SBT}}=\cos\gamma_T$, $w_{x_{SBT}}=jk_T\cos(\gamma_T-\mu_T)$, $p_{y_{SBT}}=(p-\tilde{p})d_{Ty}/\lambda+(q-\tilde{q})d_{Ry}(R_{t1}+0.5(R_{t2}-R_{t1}))/D\lambda$, $q_{y_{SBT}}=\sin\gamma_T$, $w_{y_{SBT}}=jk_T\sin(\gamma_T-\mu_T)$, $A_{SBR}=(2\pi p_{x_{SBR}}q_{x_{SBR}}+2\pi p_{y_{SBR}}q_{y_{SBR}}+w_{x_{SBR}})/2\pi f_{R\max}$, $B_{SBR}=k_R\sin(\mu_R-\gamma_R)+j2\pi p_{x_{SBR}}q_{y_{SBR}}-j2\pi p_{y_{SBR}}q_{x_{SBR}}$, $p_{x_{SBR}}=(q-\tilde{q})d_{Rx}/\lambda$, $q_{x_{SBR}}=\cos\gamma_R$, $w_{x_{SBR}}=-jk_R\cos(\gamma_R-\mu_R)$, $p_{y_{SBR}}=(q-\tilde{q})d_{Ry}/\lambda+(p-\tilde{p})d_{Ty}(R_{r1}+0.5(R_{r2}-R_{r1}))/D\lambda$, $q_{y_{SBR}}=\sin\gamma_R$, $w_{y_{SBR}}=-jk_R\sin(\gamma_R-\mu_R)$, and $I_{SBT/SBR}=[(3-2\gamma R_{t2/r2}/D)R^2_{t2/r2}-(3-2\gamma R_{t1/r1}/D)R^2_{t1/r1}]/3(R^2_{t2/r2}-R^2_{t1/r1})$. Using similar reasoning as above, the sD-psd of the double-bounced component becomes

$$\mathcal{F}_{\Delta t}\{R^{DB}_{pq,\tilde{p}\tilde{q}}(d_T,d_R,\Delta t,0)\}=\frac{\eta_{TR}I_{DB}}{I_0(k_T)I_0(k_R)} \tag{21}$$
$$\times\quad e^{j(2\pi p_{x_{DB}}q_{x_{DB}}+2\pi p_{y_{DB}}q_{y_{DB}}-jk_T\cos(\mu_T-\gamma_T))\nu/f_{T\max}}$$
$$\times\quad\frac{\cos\left(\frac{2\pi}{\lambda}\beta_{T_m}d_{Tz}\right)}{1-\left(\frac{4\beta_{T_m}d_{Tz}}{\lambda}\right)^2}\frac{\cosh\left[B_{DB}\sqrt{1-(\nu/f_{T\max})^2}\right]}{\pi f_{T\max}\sqrt{1-(\nu/f_{T\max})^2}}$$
$$\odot\quad e^{j(2\pi p_{z_{DB}}q_{z_{DB}}+2\pi p_{w_{DB}}q_{w_{DB}}-jk_R\cos(\mu_R-\gamma_R))\nu/f_{R\max}}$$
$$\times\quad\frac{\cos\left(\frac{2\pi}{\lambda}\beta_{R_m}d_{Rz}\right)}{1-\left(\frac{4\beta_{R_m}d_{Rz}}{\lambda}\right)^2}\frac{\cosh\left[C_{DB}\sqrt{1-(\nu/f_{R\max})^2}\right]}{\pi f_{R\max}\sqrt{1-(\nu/f_{R\max})^2}},$$

where $\odot$ denotes convolution, $p_{x_{DB}}=(p-\tilde{p})d_{Tx}/\lambda$, $q_{x_{SBT}}=\cos\gamma_T$, $p_{y_{DB}}=(p-\tilde{p})d_{Ty}/\lambda$, $q_{y_{SBT}}=\sin\gamma_T$, $p_{z_{DB}}=(q-\tilde{q})d_{Rx}/\lambda$, $q_{z_{DB}}=\cos\gamma_R$, $p_{w_{DB}}=(q-\tilde{q})d_{Ry}/\lambda$, $q_{w_{DB}}=\sin\gamma_R$, $|\nu|\le f_{T\max}+f_{R\max}$, $I_{DB}=(R^2_{t2}-R^2_{t1})(0.5R^2_{r2}-\gamma R^3_{r2}/(3D)-0.5R^2_{r1}+\gamma R^3_{r1}/(3D))+(R^2_{r2}-R^2_{r1})(0.5R^2_{t2}-\gamma R^3_{t2}/(3D)-0.5R^2_{t1}+\gamma R^3_{t1}/(3D))$, $B_{DB}=k_T\sin(\mu_T-\gamma_T)+j2\pi p_{x_{DB}}q_{y_{DB}}-j2\pi p_{y_{DB}}q_{x_{DB}}$, and $C_{DB}=k_R\sin(\mu_R-\gamma_R)+j2\pi p_{z_{DB}}q_{w_{DB}}-j2\pi p_{w_{DB}}q_{z_{DB}}$. By calculating the Fourier transformation of the space-time correlation

function in (18), we obtain the sD-psd of the LoS component:

$$\mathcal{F}_{\Delta t}\{R^{LoS}_{pq,\tilde{p}\tilde{q}}(d_T, d_R, \Delta t, 0)\} = \sqrt{K_{pq}K_{\tilde{p}\tilde{q}}} \quad (22)$$
$$e^{j\frac{2\pi}{\lambda}[(p-\tilde{p})d_{Tx}-(q-\tilde{q})d_{Rx}]}\delta(\nu + f_{T\max}\cos\gamma_T - f_{R\max}\cos\gamma_R),$$

where $\delta(\ \cdot\ )$ denotes the Dirac delta function. Finally, the sD-psd between two time-variant transfer functions $T_{pq}(t, f = 0)$ and $T_{\tilde{p}\tilde{q}}(t, f = 0)$ becomes a summation of the sD-psds in (19) - (22).

V. Simulation Results

In this section, we present some simulation results to verify theoretical derivations. Figs. 2 and 3 show the sD-psds for several MIMO systems. Here, we analyze the radio propagation in outdoor M-to-M micro- and macro-cells, assuming 3-D non-isotropic scattering ($k_T = k_R = 2$ for curves in Fig. 2 and $k_T = k_R = 9$ for curves in Fig. 3) and line-of-sight ($K = 2$) conditions between the $\mathrm{T_x}$ and $\mathrm{R_x}$. In all simulations we use the following parameters: $\beta_{Tm} = \beta_{Rm} = 15°$, $\theta_T = \theta_R = \pi/4$, $\psi_T = \psi_R = \pi/3$, $\gamma_T = \gamma_R = 0$, $\mu_T = 0$, $\mu_R = \pi$, $\lambda = 0.3$ m, $R_{t1} = R_{r1} = 30$ m, $R_{t2} = R_{r2} = 300$ m, $D = 10$ km, $\gamma = 4$, $L_t = L_r = 2$, $d_T = d_R \in \{0, 0.5\lambda,\ 1\lambda,\ 2\lambda\}$, and $f_{T\max} = f_{R\max} = 400$ Hz. Fig. 2 assumes that the single-bounced rays bear more energy than the double-bounced rays, i.e., $\eta_T = \eta_R = 0.3$ and $\eta_{TR} = 0.4$, which is characteristic for the outdoor M-to-M micro-cell propagation. We can observe that this spectrum is similar to the U-shaped spectrum of F-to-M cellular channels. Fig. 3 considers the macro-cell propagation (i.e. $\eta_T = \eta_R = 0.0001$ and $\eta_{TR} = 0.9998$). In this case, the sD-psd differs from the U-shaped spectrum of cellular channels. Finally, Figs. 2 and 3 compare our theoretical Doppler spectra obtained for $d_T = d_R = 0$ with measured Doppler spectra for SISO system. The measured results are taken from Figs. 4(b) and 4(d) of [5]. The close agreement between the theoretical and empirical curves confirms the utility of the proposed wideband model.

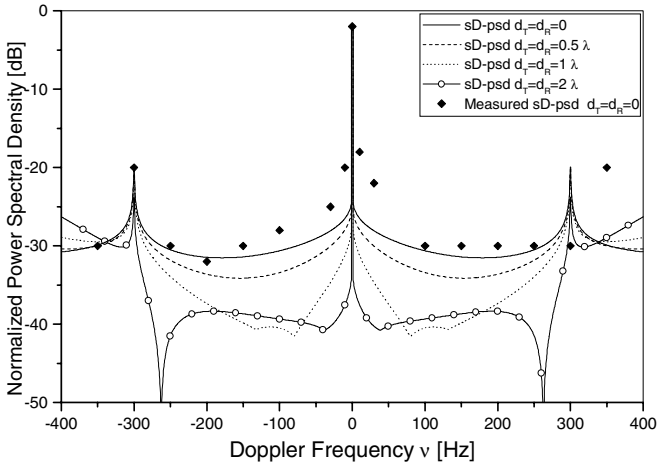

Fig. 2. The theoretical and measured sD-psd characteristic for the outdoor M-to-M micro-cells.

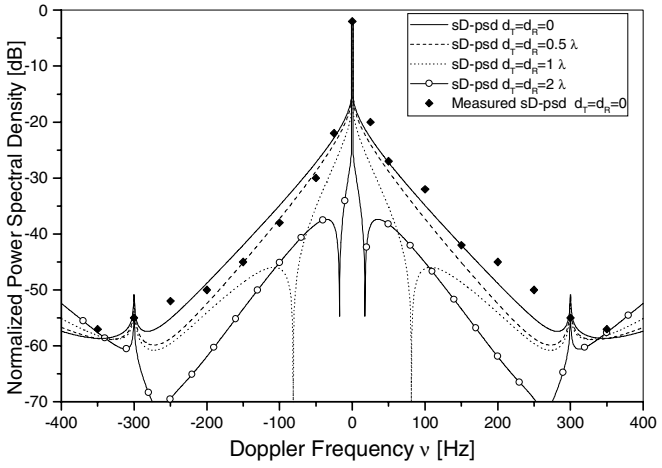

Fig. 3. The theoretical and measured sD-psd characteristic for the outdoor M-to-M macro-cells.

VI. Conclusions

This paper introduced a "concentric-cylinders" geometrical propagation model. Based on this geometrical model, a 3-D parametric reference model for wideband MIMO M-to-M fading channels was proposed. From the reference model, the space-time-frequency correlation function and space-Doppler power spectral density were derived for a 3-D non-isotropic scattering environment. Finally, simulation results for the sD-psd compare very well with measured data in [5].

Disclaimer

The views and conclusions contained in this document are those of the authors and should not be interpreted as representing the official policies, either expressed or implied, of the Army Research Laboratory or the U. S. Government.

References

[1] A.S. Akki and F. Haber, "A statistical model for mobile-to-mobile land communication channel," *IEEE Trans. on Veh. Tech.*, vol. 35, pp. 2–10, Feb. 1986.

[2] M. Pätzold, B.O. Hogstad, N. Youssef, and D. Kim, "A MIMO mobile-to-mobile channel model: Part I-the reference model," *Proc. IEEE PIMRC'05*, vol. 1, pp. 573–578, Germany, Sept. 2005.

[3] A.G. Zajić and G.L. Stüber, "Space-Time Correlated MIMO Mobile-to-Mobile Channels," *Proc. IEEE PIMRC'06*, Finland, Sept. 2006.

[4] A.G. Zajić and G.L. Stüber, "A Three-Dimensional MIMO Mobile-to-Mobile Channel Model," *IEEE WCNC'07*, Hong Kong, Mar. 2007.

[5] G. Acosta, K. Tokuda, and M. A. Ingram, "Measured joint Doppler-delay power profiles for vehicle-to-vehicle communications at 2.4 GHz," *Proc. IEEE GLOBECOM'04*, vol. 6, pp. 3813–3817, Dallas, TX, Nov. 2004.

[6] D. Gesbert, H. Bölcskei, D.A. Gore, and A.J. Paulraj, "Outdoor MIMO wireless channels: models and performance prediction," *IEEE Trans. on Commun.*, vol. 50, pp. 1926–1934, Dec. 2002.

[7] A. Abdi, J. A. Barger, and M. Kaveh, "A parametric model for the distribution of the angle of arrival and the associated correlation function and power spectrum at the mobile station," *IEEE Trans. on Veh. Tech.*, vol. 51, pp. 425–434, May 2002.

[8] J.D. Parsons and A.M.D. Turkmani, "Characterisation of mobile radio signals: model description," *IEE Proc. I, Commun., Speach, and Vision*, vol. 138, pp. 549–556, Dec. 1991.

[9] A. Kuchar, J.-P. Rossi, and E. Bonek, "Directional macro-cell channel characterization from urban measurements," *IEEE Trans. on Antennas and Propagation*, vol. 48, pp. 137–146, Feb. 2000.

[10] I.S. Gradshteyn and I.M. Ryzhik, *Table of Integrals, Series, and Products* 5^{th} *ed.*. A. Jeffrey, Ed. San Diego CA: Academic, 1994.